津波漂流物に相当する衝撃荷重を受けるコンクリート充填鋼管部材の応答特性に関する予備的実験

エフェンデイ，マハムドコリ
九州大学大学院人間環境学府空間システム専攻 ： 博士後期課程

財津，周平
九州大学大学院人間環境学府空間システム専攻 ： 博士後期課程

松尾，真太朗
九州大学大学院人間環境学研究院都市・建築学部門

河野，昭彦
九州大学大学院人間環境学研究院都市・建築学部門

https://doi.org/10.15017/1462168

出版情報：都市・建築学研究. 24, pp.97-106, 2013-07-15. Faculty of Human-Environment Studies, Kyushu University
バージョン：
権利関係：

都市・建築学研究　九州大学大学院人間環境学研究院紀要　第24号，2013年7月
J. of Architecture and Urban Design, Kyushu University, No.24, pp.97～106, July. 2013

津波漂流物に相当する衝撃荷重を受けるコンクリート充填鋼管部材の応答特性に関する予備的実験

A Preliminary Test on Response Characteristics of Concrete-Filled Tubular Specimens under Impact Loads Corresponding to Tsunami Flotsam

エフェンディマハムドコリ*，財津周平*，松尾真太朗**，河野昭彦**
Mahmud Kori EFFENDI*, Shuhei ZAITSU*, Shintaro MATSUO** and Akihiko KAWANO**

In this study, impact loading tests of six specimens were conducted using the falling weight impact loading machine in order to get the basic knowledge on the response characteristics of concrete-filled steel tubular (CFT) specimens. Although the maximum velocity of Tsunami might be estimated as 15m/s in typical seashore, it may be thought that around 7m/second is the maximum velocity of the flotsam in inland. The impact velocity of falling weight is proportional to the square root of the falling height of the weight, so that the maximum falling height in this test is determined as 2.5m corresponding to the velocity of 7m/s. Another four specimens were also conducted under static condition which are the standard references to be compared with the specimens subjected to impact loads. The specimens are simply-supported beams, and the impact loads or static loads concentrically and vertically applies to the mid-span of the beams. The test specimens are circular and square CFT specimens and circular and square vacant steel tubular specimens. The increase of heaviness and velocity of the weight increase the plastic energy dissipation and the input energy for specimens. As the result of impact loading test, the CFT specimens could sustain much higher levels of the heaviness and velocity of falling weight than those of vacant steel tubular specimens.

Keywords: Concrete Filled Steel Tubular Specimens, Impact Loading Test, Absorbed energy, Tsunami Flotsam
コンクリート充填鋼管部材，衝撃試験，吸収エネルギー，津波漂流物

1. Introduction

Tohoku district-off the Tohoku- Offshore Pacific Ocean Earthquake (magnitude 9.0 (Mw)) which occurred on March 11th, 2011 brought about serious human life and property damage by the earthquake motion or Tsunami. Tsunami hit over the wide range areas of the Pacific coast of East Japan, such as Iwate Prefecture, Miyagi Prefecture, Fukushima Prefecture, and Chiba Prefecture.

Many people were dead and almost 18,000 people were missing[1,2] because of this large-size Tsunami. The effect of this Tsunami is more destructive than that of the Sanriku Tsunami by the 1933 Sanriku earthquake, and that of Tsunami by the central Sea of Japan earthquake in May, 1983. This earthquake and Tsunami also caused extensive and severe structural damage in north-eastern Japan.

Lessons can be learned from the past Tsunami damage such as provision of good early warning and vertical evacuation systems which it can help refuge in a certain time immediately after the official announcement of Tsunami warning.

In the provisional guideline[3], description of the requirements of the Tsunami evacuation building has been attached, in which, evacuation building, regardless of the type of structure, should be built by wood structure, steel frame structures and reinforced concrete (RC) structure. Design examples of six, eight, and ten stories at the most buildings with inundation depth of 15m are shown.・It is shown in the provisional guideline that the Tsunami wave pressure is largely predictable. Although the flow rate can be estimated roughly by the inundation depth, but mass and collision direction of Tsunami flotsams contain a stochastic problem. If the large mass of the flotsam collides with a large building, it could create serious damage such as collapse. The aim of this study was to get basic knowledge of the CFT and vacant tubular specimens' behavior under static and impact loads corresponding to Tsunami flotsam. Energy principle is used to estimate the magnitude of impact load of the test specimens.

2. Overview of experiment

2.1 Flow velocity of Tsunami flotsam

The hydrodynamic forces estimation applied to

* Department of Architecture
空間システム専攻博士後期課程
** Department of Architecture and Urban Design
都市・建築学部門

structures during a Tsunami can be estimated by the flow depth and the Tsunami velocity. It has been reported that the Tsunami flotsam velocity has been left unresolved. In addition, at the time of Tohoku- Offshore Pacific Ocean Earthquake, the estimated Tsunami velocity from the video analysis in the riverbank area in Natori, Miyagi Prefecture has been reported to 7m/s and (25km/h) [1]. The following formula has been proposed as one of the estimation formula of the Tsunami velocity in inland [4,5].

$$u = 1.1\sqrt{gh_f} \tag{1}$$

$$u = 2.0\sqrt{gh_r} \tag{2}$$

Here, u is onshore Tsunami flow velocity, g is acceleration due to gravity, h_f is inundation depth at the front of the building and h_r is inundation depth at the back of the building.

Table 1. Mechanical Properties

Cross Section	Circle	Square
Type	STK400	STKR400
Yield Stress, ${}_s\sigma_y$ (N/mm²)	450	415
Young Modulus (E) (N/mm²)	1.85x10⁵	1.9x10⁵
Yield Strain (%)	0.24	0.21
Concrete Strength (${}_c\sigma_{cB}$) (N/mm²)	73.8	

Table 2. Test specimen data

Specimen	Tubes	D (mm)	t mm)	Span (L) (mm)	Experimental Method	Falling Height (H) (m)	Falling Weight (M) (kg)
Cf1	Circular CFT	101.7	2.97	900	Impact	1.00	79.1
						1.75	
						2.50	
Cf2					Impact	2.50	79.1
							167.7
Cf3					Static	-	-
Cv4	Circular Vacant				Impact	1.00	79.1
Cv5					Static	-	-
Sf1	Square CFT	100.3	2.97	625	Impact	1.00	79.1
						1.00	
						1.00	
						1.75	
						2.50	
				900		2.50	167.7
Sf2				900	Impact	2.50	79.1
							167.7
Sf3					Static	-	-
Sv4	Square Vacant				Impact	1.00	79.1
						1.25	
Sv5					Static	-	-

Note : D=outside diameter of the tube, t=thickness of the tube

From the two equations above, changing the Tsunami inundation flow depth in the front and back of the building also changes the Tsunami velocity. Tsunami velocity was typically found in the range from 5 to 8 m/s [6].

The Tsunami flow velocity is made in general into the same as 7 m/s, and Tsunami flotsam velocity as well. If there is no significant friction and no other energy stored in the impact test apparatus, at the point of collision, the kinetic energy is simply the potential energy lost by the falling weight.

The falling height of the weight, H is calculated by velocity, v:

$$H = \frac{v^2}{2g} \tag{3}$$

Here, H=2.5m for v=7m/s.

2.2 Index of impact load

When collision velocity is 10 m/s or less, it is called as a low-speed impulse load problem. Tsunami flotsam may hit building with velocity of this. Input energy is considered appropriate as an indicator of the damage of structural specimens against Tsunami flotsam impact load.

So, if the balance of the following energy has occurred, it will follow:

$$E_I = E_E + E_V + E_{LP} + E_{OP} \tag{4}$$

Here, E_I is input energy due to impact load, E_E is elastic strain energy or elastic vibration energy, E_V is stress wave propagation attenuation due to energy absorption, E_{LP} is absorbed energy by the local plastic deformation in a pointed impact-load pressure, E_{OP} is absorbed energy by the plastic deformation of the entire specimens.

E_V are difficult to be evaluated. According to the Deng et. al.[7], it is shown that the following handling is possible.

$$\beta E_I \cong E_E + E_{LP} + E_{OP} \tag{5}$$

Here, β on E_I is the reduction rate of the energy input by ignoring the arrows. It is about 0.75 according literature[7]. The energy balance of a member denoted by a formula (5), and will be clarified by the experiment.

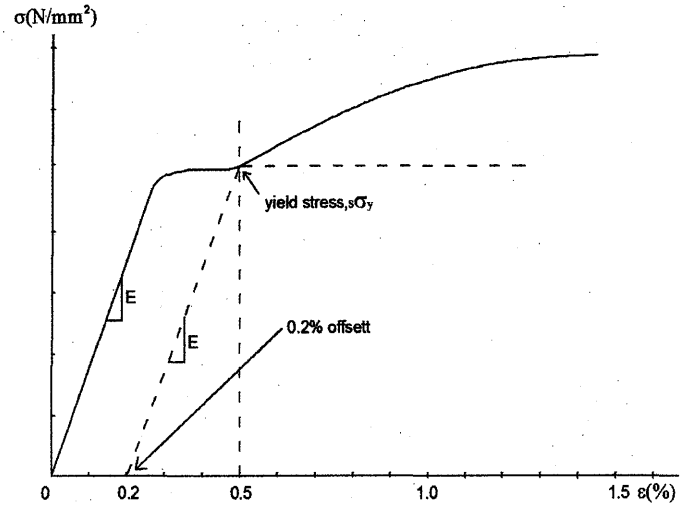

Fig.1 Initial Part of Stress-Strain Curve for High Strength Steel

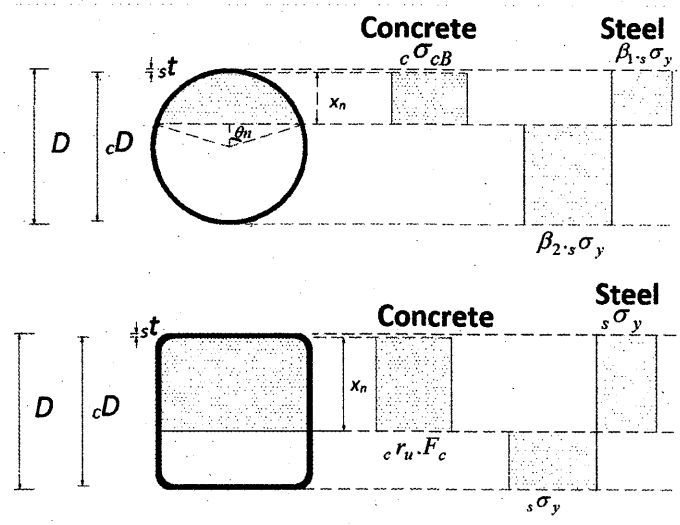

Fig.2 Stress Block for ultimate bending capacity

2.3 Specimens and experimental parameters

2.3.1 Specimens and mechanical properties

The tensile strength of the steel tubes was tested under conditions specified in Japanese Industrial Standards (JIS). The samples were taken from the faces of the square and circle vacant tubular specimens. From Fig. 1 the yield strength is defined as 0.2% offset value. A line parallel to the first part of the stress-strain curve is constructed then offset by 0.2% from the origin. Young's modulus, E_s, is the ratio of stress to strain within the elastic region of the stress and strain curve. The yield strain is calculated as follow:

$$\varepsilon_y = \frac{{}_s\sigma_y}{E_s} \tag{6}$$

Where, ${}_s\sigma_y$ is the mean yield strength, and ε_y is the yield strain.

For the circular section, ${}_s\sigma_y$ was 450 N/mm² and ε_y was 0.24%. For the square section, ${}_s\sigma_y$ was 415 N/mm² and ε_y was 0.21%. The material properties can be seen in Table 1. The unconfined compressive strength of the concrete was an average value of 73.8 N/mm² at the four weeks after casting of concrete.

Impact loading tests of six specimens were conducted using the falling weight impact loading machine. Another four specimens were tested under static loading condition. The test specimens consist of both concrete infill and vacant of circular and square tubular specimens. The test specimen's detail can be seen in Table 2. Specimen Cf1 and Sf1 are tested under impact loads from 1m, 1.75m, to 2.5m falling weight height, respectively. Cf2 and Sf2 are tested with direct impact load, 2.5m falling weight height.

2.3.2 Ultimate strength of specimens

The theoretical value of ultimate moment capacity for the static testing specimens based on the stress distributions shown in Fig. 2 with the neutral axis at a distance x_n from the extreme compression fiber. The calculation procedure is as follows[8]: The neutral axis position is obtained by setting the total of axial force equal to zero and the ultimate moment capacity is calculated.

$$N_u = {}_cN_u + {}_sN_u \tag{7}$$

$$M_u = {}_cM_u + {}_sM_u \tag{8}$$

The strengths appearing on the right sides are given as follow:

For square CFT beam-column:

$${}_cN_u = x_{n1}\cdot{}_cD^2\cdot{}_cr_u.F_c \tag{9}$$

$${}_cM_u = \frac{1}{2}(1-x_{n1})x_{n1}\cdot{}_cD^3\cdot{}_cr_u.F_c \tag{10}$$

$${}_sN_u = 2(2x_{n1}-1)\cdot{}_cD\cdot{}_st\cdot{}_s\sigma_y \tag{11}$$

$${}_sM_u = \left[\left[1-\frac{{}_st}{D}\right]D^2 + 2[1-x_{n1}]x_n\cdot{}_cD\right]{}_st\cdot{}_s\sigma_y \tag{12}$$

For circular CFT beam-column:

$${}_cN_u = (\theta_n - \sin\theta_n\cos\theta_n).\frac{{}_cD^2\cdot{}_c\sigma_{cB}}{4} \tag{13}$$

$${}_cM_u = \sin^3\theta_n.\frac{{}_cD^3\cdot{}_c\sigma_{cB}}{12} \tag{14}$$

$${}_sN_u = \{\beta_1\theta_n + \beta_2(\theta_n - \pi)\}\left(1-\frac{{}_st}{D}\right).D\cdot{}_st\cdot{}_s\sigma_y \tag{15}$$

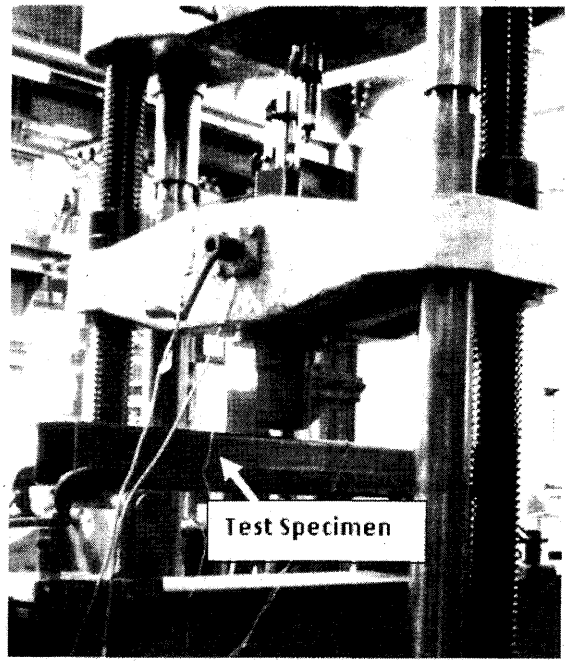

Fig. 3 Static Loading Test Apparatus

$$ {}_sM_u = (\beta_1 + \beta_2)\sin\theta_n \frac{\left(1-\frac{{}_st}{D}\right)^2}{2} . D^2 \cdot {}_st \cdot {}_s\sigma_y \quad (16) $$

Where,

$$ x_{n1} = \frac{x_n}{{}_cD} \quad (17) $$

$$ \theta_n = \cos^{-1}(1-2x_{n1}) \quad (18) $$

$$ \beta_1 = 1 \ , \ \beta_2 = 1 \quad (19) $$

Where, N_u is ultimate axial load, M_u is ultimate bending moment, ${}_cN_u$ is ultimate axial load of concrete, ${}_sN_u$ is ultimate axial load of steel, ${}_cM_u$ is ultimate moment of concrete, ${}_sM_u$ is ultimate moment of steel, D is width or diameter of a steel tube section, ${}_cr_u$=0.85 is reduction factor for concrete strength, ${}_cD$ is width or diameter of a concrete section, ${}_st$ is thickness of a steel tube section, x_n is position parameter of neutral axis, and ${}_s\sigma_y$ is yield stress of steel tube, ${}_c\sigma_{cB}$ is the strength increase of confined concrete, F_c is design standard strength of infill concrete.

The M_u calculated from Eg. (7) to (19) is regarded as the CFT full plastic moment, M_p, taking the account of axial force effect.

For vacant steel tubular specimen:

$$ M_p = {}_s\sigma_y Z_p \quad (20) $$

Where Z_p is the plastic modulus of a cross-section, and ${}_s\sigma_y$ is the yield stress of a steel tube.

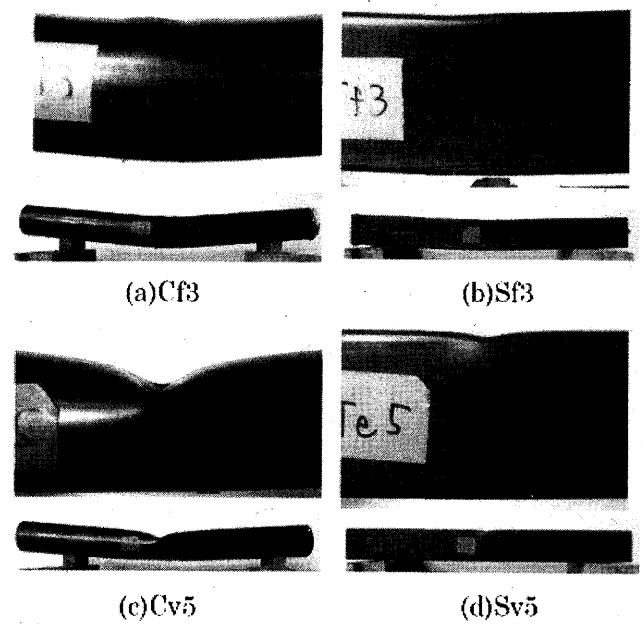

Fig. 4 Static Failure Modes of circular CFT (Cf3), square CFT (Sf3), circular vacant tube (Cv5) and square vacant tube (Sv5)

3. Static test program

3.1 Test apparatus

The static loading test apparatus is shown in Fig. 3. The tip of the loading point is made the same as that of impact loading test. The specimens are simply supported beam with the pin and roller supports. Lateral load is resulted by 500 kN capacity testing machine. The incremental loads are applied until reaching the strength reduction of the test specimens. The mid-span deflection is recorded by a laser displacement sensor. Strain gauges are located on underside of the mid span of test specimen and upper-side of 100 mm right and left from the mid-span of the test specimen.

3.2 Static test results

The following section summarizes the results of the static test experiments.

3.2.1 Plastic deformation and local failure

Steel structure can fail by brittle or ductile failure after they undergo plastic deformation. The structures undergo large plastic deformation can provide a large reserve of strength. The final failure of test specimen is local indentation and global specimens bending. The effect of infill concrete in reducing the local damage of the specimens are clearly shown in Fig. 4.

3.2.2 Load-deflection relationships

The relationships between the applied load and the mid-span deflections of the four static test specimens are shown in Fig. 5. It shows the maximum load of Cf3, Cv5, Sf3 and Sv5 are 80.9 kN, 29.1 kN, 109.2 kN, and 44. 1 kN, respectively. Figure 5 shows that the circular CFT and

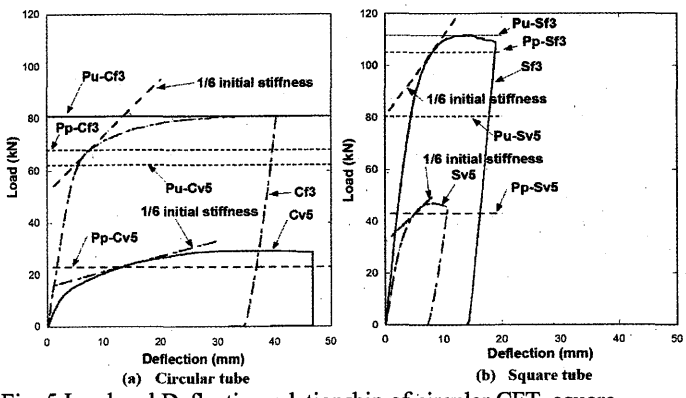

Fig. 5 Load and Deflection relationship of circular CFT, square CFT and vacant tubular members

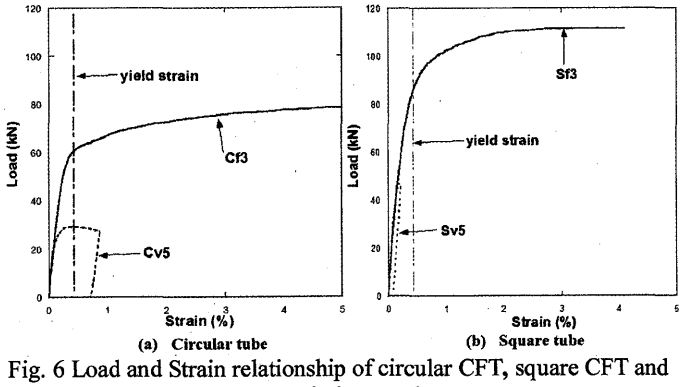

Fig. 6 Load and Strain relationship of circular CFT, square CFT and vacant tubular members

Table 3. Requirement of energy for plastic deformation

Cross Section	Circular Member		Square Member	
	Vacant Tubes	CFT	Vacant Tubes	CFT
M_p(kNm)	14.0	18.2	18.1	25.1
P_p (kN)	62.0	80.9	80.6	111.6
E_{OP} (Joule)	2790	3640	3627	5020

vacant tubular specimens exhibited relatively constant deflection at near maximum load compared with the square CFT and vacant tubular specimens. It provides sufficient warning before the specimen reach global failure.

The fully plastic load, (P_p), is determined from the experimental results by horizontal projection of point of contact between load-deflection relationship curve and one-sixth of initial stiffness of the specimens (Fig.4).

3.2.3 Load-bending strain relationships in tension sides of cross sections

Figure 6 shows the relationship between mid-span tension side strain and applied load. It shows that the square CFT section has higher yield, plastic and ultimate load compared with circular CFT section. The square vacant specimen has shorter plastic deformation than that of circular vacant specimen.

Figure 6 shows that the tensile strain of Sv5 doesn't

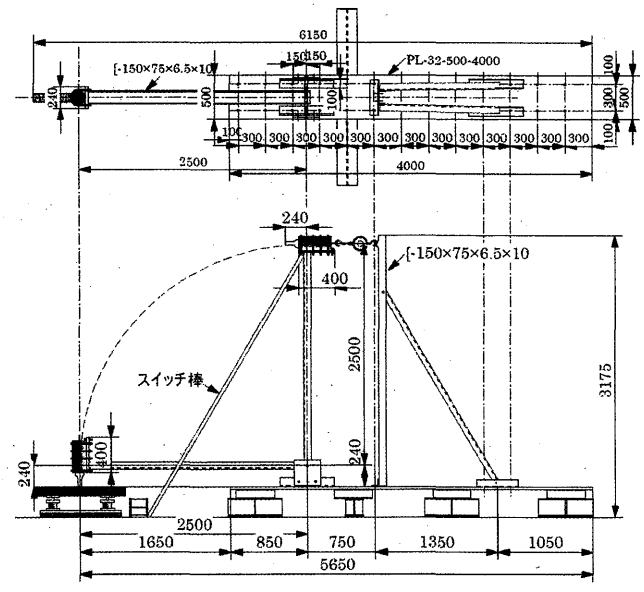

Fig. 7 Impact Loading Test Apparatus

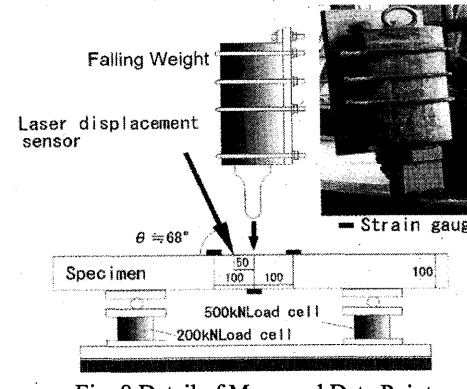

Fig. 8 Detail of Measured Data Point

increase after reaching the maximum static load. It seems that the specimens show local deformation at point of the static loading. It shows that the tensile strain keeps in constant value, but the deflection still increase because of local failure in compression side of cross-section.

4. Impact test program

4.1 Test apparatus

Figure 7 shows the impact loading test apparatus which can be divided into frame on which steel channel holding the falling weight, base plate and falling weight assembly. The impact loading test apparatus consists of a 79.1 kg or 167.7 kg falling weight assembly being struck at a height from 1000mm, 1750mm to maximum height of 2500 mm, respectively. The 2500 mm height of falling weight is corresponding to Tsunami flow velocity of 7 m/s. The supporting conditions of a test specimen were pin and roller support. The span length of the test specimen is 900 mm.

The hemispherical falling weight tip has a diameter of 40 mm and 150mm length. The tip's material must be much

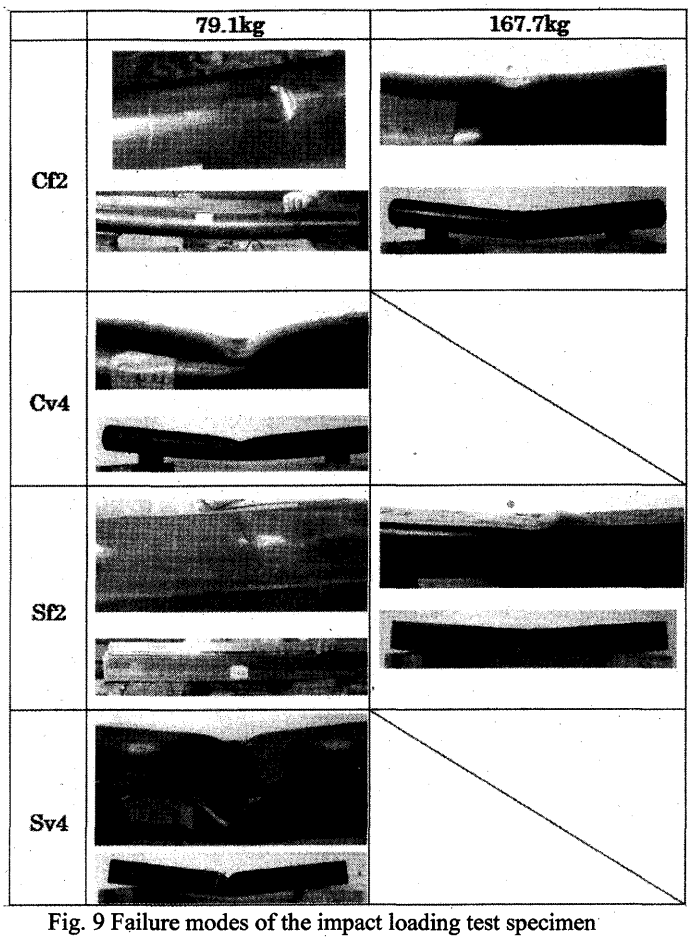

Fig. 9 Failure modes of the impact loading test specimen

harder than test specimens' material so that the yield stress is larger than 450 N/mm^2 and furthermore the quenching process was done. The tip is attached to the cylinder rod with diameter of 200 mm and 370 length.

The falling weight tip used hemispherical shape because the stress wave caused by the hemispherical falling weight may have propagated more uniformly owing to the progressive contact between the falling weight and the top face of the test specimens[9].

The falling weight masses should be greater than the test specimens because the recorded impact load–time relationship might be hard to interpret because of the mutual excitation of the two masses and the resulting presence of inertial and harmonic oscillations[10].

Figure 8 shows the location to measure impact response data of the test specimen. Mid span deflection is measured by a laser displacement sensor. Support reaction forces are measured by load cells at both ends. Strain gauges are located on underside of the mid span of test specimens and upper-side of 100 mm right and left side from the mid-span of the test specimens.

Figure 8 shows the falling weight can be clamped and be released to certain masses related to the desired impact

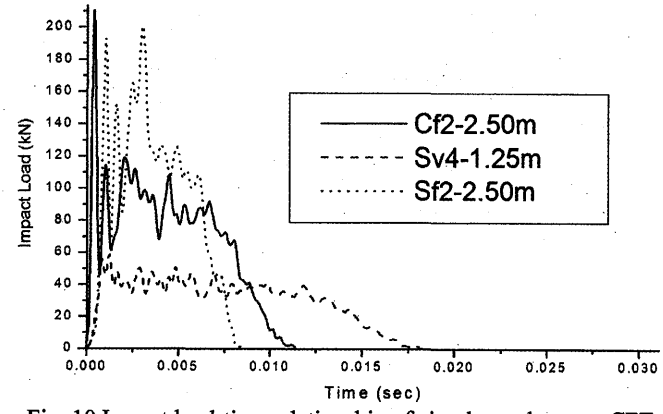

Fig. 10 Impact load-time relationship of circular and square CFT and square vacant tubular members

velocity. The falling weight is assumed moving together with the same velocity as the test specimens after the collision. The maximum falling weight height is 2.5 m which corresponds to a maximum impact velocity of 7 m/s.

4.2 Test results

The signal data recorded by the data acquisition system are complex which include the effect of inertial loading of the tip, test specimens and support system, low-frequency fluctuations, and high-frequency noise. Hence, the support force-time signals obtained from data acquisition are not the indicative of the impact load of the test specimens. Because of difficulty in acquiring data from the falling weight part, summation of the support reactions are used as impact load. When determining impact load magnitudes, the raw data from the recorded load time relationship is generally used[11].

The following section summarizes the results of the impact test experiments.

4.2.1 Failure modes

All the specimens failed on the vicinity of a loading point where the impact struck the testing specimen before global failure occurred. The effect of infill concrete in both circular and square tubular sections greatly enhanced the resistance for the local failure. Figure 9 clearly shows the difference in local failure between the vacant tubular and CFT specimens.

4.2.2 Mass requirement for impact loading test

The destruction of the specimen is defined as when the plastic rotation angle of test specimens exceed a certain limit so the tensile stress is most prominent in the middle of the test specimens. The plastic rotation angle of the test specimens are defined about 10% of the span length correspond to buildings damaged by earthquake, the residual story drift angle over 3% is judged as collapse, according to the Japan Building Disaster Prevention Association. In this case, the energy due to elastic deformation and damping are

Tale 4. Comparison between theoretical and experimental full plastic load

Cross Section	Testing Name	Experimental	Calculation		Ratio of (1) / (2)
		$_eP_p$ (kN) (1)	M_p (kNm)	P_p (kN) (2)	
Circular CFT	Cf3	70.4	18.2	80.9	0.87
Circular Vacant Tubes	Cv5	23.4	14.0	62.0	0.38
Square CFT	Sf3	104.3	25.1	111.6	0.93
Square Vacant tubes	Sv5	42.6	18.1	80.6	0.53

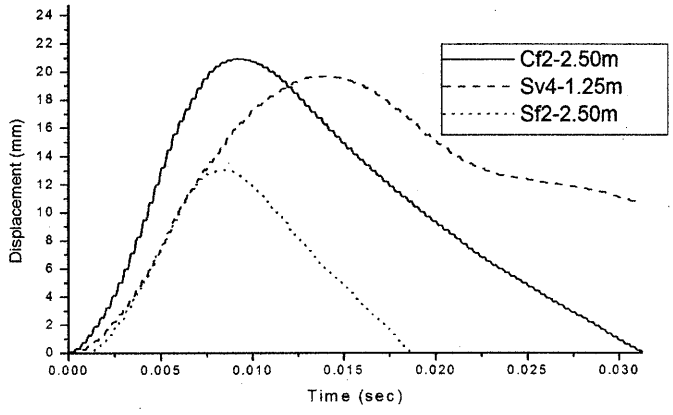

Fig. 11 Dispacement-time relationship of circular and square CFT and square vacant tubular members

small, and the absorbed energy by the plastic deformation of the specimens occupy most. Then, absorbed energy of the entire collapse E_{OP} is defined by:

$$E_{OP} = P_p(0.05L) \tag{21}$$

$$P_p = \frac{4Mp}{L} \tag{22}$$

Where, L = 900 mm is the span of the specimen, P_p is plastic collapse load of a specimen.

The mass of the falling weight has to be large enough so that a specimen deforms plastically. The required mass m_n, which corresponds to E_{OP} at specified falling height H, is derived from the following equation.

$$m \cong \frac{E_{OP}}{gH} \tag{23}$$

The calculation mass of the falling weight is 113.8 kg, 148.5 kg, 148 kg, and 204 kg for 2.5m of falling heights for Cv5, Cf3, Sv5, and Sf3 specimens, respectively. These calculated masses of falling weight were taken into account in the real experiment.

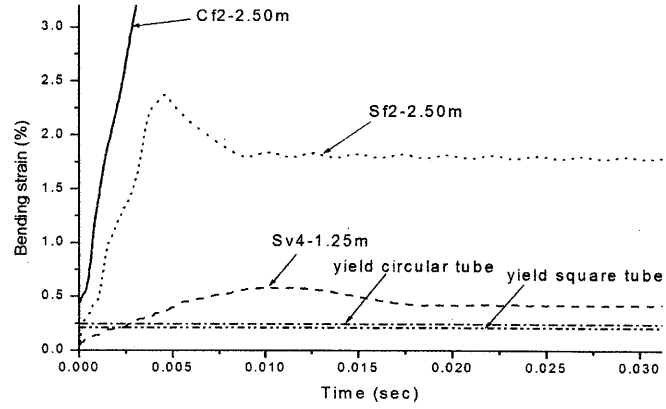

Fig. 12 Bending strain-time relationship of circular CFT and square CFT and square vacant tubular members

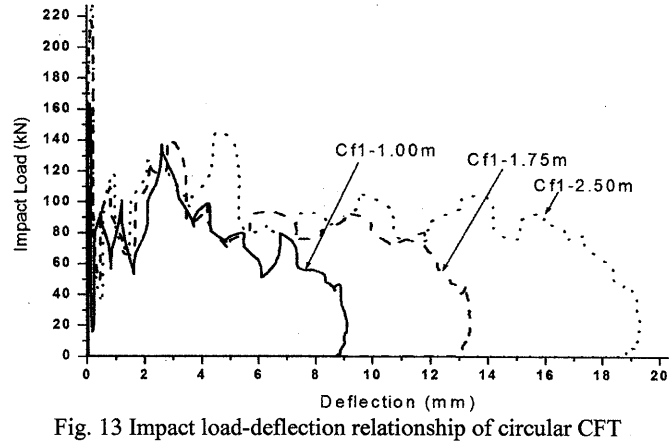

Fig. 13 Impact load-deflection relationship of circular CFT members at various falling height of a weight

4.2.3 Time history of impact load responses

Figure 10 shows impact load and time relationship for circular CFT (Cf2), square vacant tubes (Sv4) and square CFT (Sf2) specimens. The impact load was evaluated by summing the values from both reaction forces at both end supports. The loading period of the impact of CFT specimens is shorter than that of vacant tube specimens probably because of the damping effect from infill concrete.

The maximum impact load at the time of collision of Sf2-2.5m, Sv4-1.25m, and Cf2-2.5m were 200 kN, 58.7 kN and 210 kN, respectively. However, those values may be very sensitive by loading conditions, supporting conditions and specimen's structural characteristics. Therefore, the absolute values can't be discussed, but CFT specimens are subjected to higher level of impact load than that of vacant tubes. It may be caused by the surface of CFT specimens which are hardened by infill concrete.

4.2.4 Time history of mid-span deflections

Figure 11 shows the deflection of the specimen at mid span obtained by laser displacement sensor. The maximum deflection of Sf2-2.5m, Sv4-1.25m, and Cf2-2.5m are 13.06 mm, 19.56 mm and 20.92 mm, corresponding to 0.01, 0.021 and 0.023 of span length, respectively. The deflection of square vacant (Sv4-1.25 m) is higher than that of square

Table 5. Energy absorption of the members

Specimen	H (m)	M (kg)	Input energy E_I (Joule) (1)	Absorbed Energy E_{OP} (Joule) (2)	E_{OP}/E_I (%)	Elactic Energy (E_E) (Joule) (3)	E_{OP}/E_E (%)
Cf1	1.00	79.1	775.0	697.0	89.9	184.0	4.2
	1.75	79.1	1357.0	1157.0	85.3	184.0	7.4
	2.50	79.1	1938.0	1770.0	91.3	184.0	10.5
Cf2	2.50	79.1	1938.0	1817.0	93.8	184.0	10.5
	2.50	167.7	4109.0	no data		no data	
Sf1	1.00	79.1	775.0	no data		no data	
	1.75	79.1	1357.0	no data		no data	
	2.50	167.7	1938.0	no data		no data	
Sf2	2.50	79.1	1938.0	1562.0	80.6	276.3	7.0
	2.50	167.7	4109.0	no data		276.3	14.9
Cv4	1.00	79.1	no data			53.9	-
	1.25	79.1	969.0	no data		53.9	18.0
Sv4	1.00	79.1	775.0	523.0	67.5	69.7	11.1
	1.25	79.1	969.0	761.0	78.5	69.7	13.9
	2.50	79.1	1938.0	no data		69.7	27.8

Table. 6 Impact and Static Load Comparison

Testing Name	Loading		Dynamic Magnification Factor (1)/(2)
	Maximum Impact Load (kN) (1)	Static Full Plastic Load (kN) (2)	
Cf3	210.0	70.4	3.0
Cv5	-	23.4	-
Sf3	200.0	104.3	1.9
Sv5	58.7	42.6	1.4

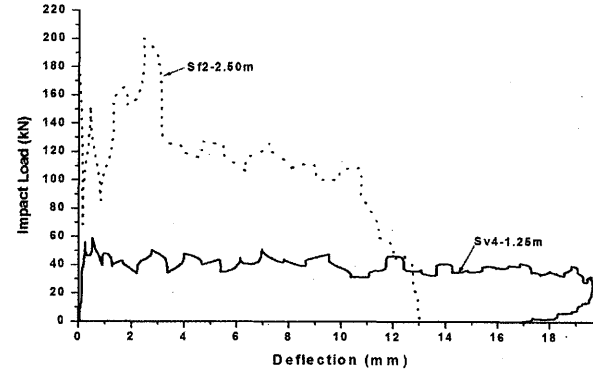

Fig.14 Impact load-midspan deflection relationship of circular and CFT specimen and square vacant tubular members

CFT (Sf2-2.5m) even though the falling height of Sv4-1.25m is smaller than Sf2-2.5m. This is because the effect of infill concrete in specimens increases the flexural strength and decreases the local deformation. The times of the end of impact load and the peak mid-span deflection are slightly different probably because of time lag of the instrument device.

4.2.5 Time history of bending strain in tension side of cross section

Figure 12 shows the bending strain at lower side of mid cross section of a specimen. The maximum permanent strain of Cf2-2.5m after 0,32% was not measured because the range of data recorder was exceeded. The maximum permanent strains of Sv4-1.25m, and Sf2-2.5m are 0,54% and 1.8%, respectively which exceed the yield strain. It can be concluded that all of the specimens yield fully during the test. The increase rate of strain in the vacant square tubular specimen Sv4 is much lower than those of CFT specimens, which may be caused by local failure at hitting point. This is because local failure in compression side of cross section.

5. Discussion

5.1 Comparison between experimental and theoretical full plastic load

A comparison between the experimental full plastic load, ${}_eP_p$, and the theoretical full plastic load, P_p, are shown in Table 4. The P_p is calculated corresponding to M_p in section 2.3.2. The confining effect of steel tube members is ignored in the calculation of full plastic load. For Circular and Square CFT specimens, although the P_p slightly overestimates the corresponding ${}_eP_p$, good agreement can be found. For circular and square vacant tubular specimens overestimate two or three times.

5.2 Energy Absorption

The input energy, E_I, can be calculated through a simple potential energy calculation using Eq. (24). Elastic energy is calculated using Eq. (25).

$$E_I = mgH \tag{24}$$

$$E_E = \frac{P_p^2}{2K} \tag{25}$$

where K is the elastic stiffness of load-deflection relation obtained by static test. The more deflection of test specimens, the greater energy required, than elastic energy.

Impact capacity is a function of the load-time and is related more closely with energy absorption than with a maximum measured load[10]. The energy absorption E_{LP} is calculated as the sum of the areas under the load deflection

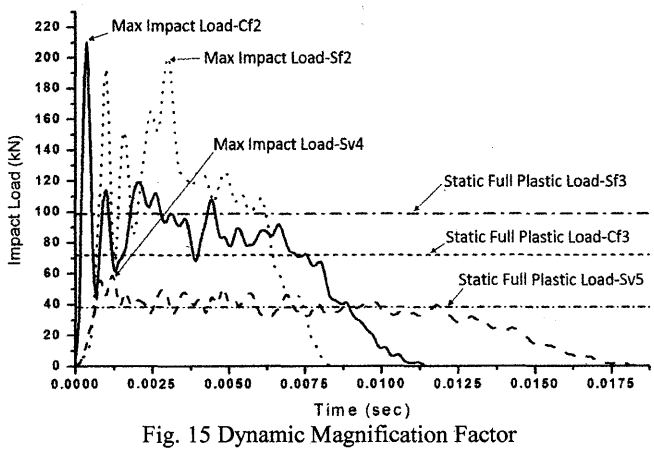

Fig. 15 Dynamic Magnification Factor

relations.

Fig. 13 shows impact load-midspan deflection relations. As the falling weight is higher, the deflection is larger. As this way, the energy absorption increases corresponding to the increase of falling weight height.

Fig. 14 shows the comparison of the impact responses between square vacant tubular specimen Sv4-1.25m and square CFT members Sf2-2.5m. It is clearly shown that infill concrete increase the impact load responses even though the differences of the falling height of a weight are considered.

Table 5 summarizes the energy absorption, E_{OP}, of the various specimens. The 167.7 kg weight is only used to investigate the damage degree of a specimen with respect to increasing weight. From Table 5, apparently all the specimens have the absorbed energy E_{OP} smaller than input energy E_I. However, CFT specimens have greater ratio of E_{OP} to E_I than those of vacant tubular specimens which may be because of local deformation.

The ratio of E_{OP} to E_I of Cf1 increases as the falling weight height increases. Either Cv4 or Sf1 results data can't be compared with other tubular specimens because no data recorded during the test.

The input energy is transformed into other form of energy as the falling weight falls (Eq.4). Square CFT and square vacant tubular specimens have a high stiffness and high full plastic load compared with circular CFT and circular vacant tubular specimens, respectively, therefore the elastic energy of square tubular specimens are higher than those of circular tubular specimens.

5.3 Comparison between the responses of impact loading and static loading

Impact load should be larger than static load. The impact factor is introduced to account for the dynamic amplification. This factor is the ratio of maximum impact load to static full plastic load. The impact factor of each specimen can be seen clearly in Fig. 15. From Table 6 shows that the impact maximum load of CFT specimen about twice of fully plastic load. For vacant square tubular member shows the maximum impact load is greater about half of fully plastic static load.

6. Conclusive Remarks

This paper has investigated experimentally the behavior of circular and square CFT and circular and square vacant tubular specimens under static and impact load corresponding to Tsunami flotsam.

Some comments about this Tsunami flotsam impact load on circular CFT, square CFT and circular and square vacant tubular specimens are worth noting:

1. All specimens were fully yielded during the experimental work.
2. The vacant tube mainly fail by local deformation at the hitting point. The effect of infill concrete in both circular and square section greatly enhanced the resistance to restrain the local deformation.
3. The higher falling height of a weight causes the longer loading period of the impact load.
4. The deflection of vacant tubular member is larger than that of CFT member, because the effect of infill concrete increases the local surface strength and the flexural strength.
5. The work in this paper provides a basis for further experimental research on the structural behavior of concrete filled steel tubular specimens against Tsunami flotsam impact loads.

7. Acknowledgement

We thank to students at Kawano laboratory, Kyushu University for helping doing impact test.

References

1) National Institute for Land and Infrastructure Management, Ministry of Land, Infrastructure, Transport and Tourism Building Research Institute, Incorporated Administrative Agency, Building Research Data No. 132 May 2011: Quick Report of the Field Survey and Research on "The 2011 off the Pacific coast of Tohoku Earthquake" (The Great East Japan Earthquake). (in Japanese)
2) Architectural Institute of Japan: Seismic hazard investigation of the 2011 Tohoku-district Pacific Ocean, July, 2011. (in Japanese)
3) Technical meeting: Ministry of Land, Infrastructure, Transport and Tourism Road Bureau, National Institute for Land and Infrastructure Management, and

Technical Research Development Result Report No.19-2 "Research on Damage Prediction and Its Mitigation Measure of the Road Structure by Tsunami" that contribute to improvement in the quality of a road policy, June, 2010 (in Japanese)
4) Hideo Matsutomi, Hidenori Iizuka: Simple Estimation Method of Tsunami Land and Its Flow rate, Proceeding of Coastal Engineering, volume 45, pp.361-365, 1998. (in Japanese)
5) Hidenori Iizuka, Hideo Matsutomi: The assessment of damage of a Tsunami flood style, coastal engineering collected papers, the 47th volume, Japan Society of Civil Engineers, pp.381-385-2000.
6) Architectural Institute of Japan: Guidelines for Design and Construction of Concrete-filled Steel Tubular Structure, in October 2008. (in Japanese)
7) Y. Deng, C. Y. Tuan and Y. Xiao: Flexural Behavior of Concrete-Filled Circular Steel Tubes under High-Strain Rate Impact Loading, Journal of Structural Engineering, Vol.138, ASCE, pp.138-449, 2012.3.
8) Morino, S and Tsuda, K: Design and Construction of Concrete-Filled Steel Tube Column System in Japan, Earthquake Engineering and Engineering Seismology, Vol. 4, No. 1, 2003
9) May, I. M., Chen, Y : Reinforced concrete members under drop-weight impacts, Proceedings of the Institution of Civil Engineers Structures and Buildings 162 Issue SB1, pp: 45-56, 2009
10) Feraboli, P. (2006). Some Recommendations for Characterization of Composite Panels by. Means of Drop Tower Impact Testing, Journal of Aircraft, Vol. 43, No. 6, pp: 1710 – 1718, 2006
11) Kelkar, A.D., Grace, C., Sankar, J., "Threshold damage criteria for thin and thick laminates subjected to low velocity impact loads", International Conference on Composites Materials ICCM 11, Paris 1999.
12) Yousuf, Mohammad et al: Experimental Behavior of Pre-compressed Concrete-filled Stainless Steel Tubular Columns Subjected to Transverse Impact Loads, 4th International Conference on Steel & Composite Structure, Sydney, Australia, July 2010
13) Norimitsu Kishi et al: An empirical Impact Resistant Design Formula of RC Beams with Statically Bending Failure Mode, Proceedings of the Japanese Society of Civil Engineers, No.647/I-51, pp.177-190, 2000.4. (in Japanese)
14) Chock, G., et al : Tohoku Tsunami-induced Building Damage Analysis Including the Contribution of Earthquake Resistant Design to Tsunami Resilience of Multi-story Buildings, International symposium on engineering lessons learned from the 2011 Great East Japan Earthquake, March 1-4, 2012
15) Tachibana, S. Masuya, H. Nakamura, S: Performance Based Design of Reinforced Concrete Beams under Impact, Natural Hazards and Earth System Science, Volume 10, Issue 6, 2010, pp.1069-1078
16) Architectural Institute of Japan (AIJ): Standard for Structural Calculation of Steel Reinforced Concrete Structures, English Ed. 1991.

（受理：平成25年5月23日）